What Controls the Optical Properties of DNA-Linked Gold Nanoparticle Assemblies?

James J. Storhoff,[‡] Anne A. Lazarides,[‡] Robert C. Mucic,[‡] Chad A. Mirkin,*[,‡] Robert L. Letsinger,*[,†] and George C. Schatz*[,‡]

Contribution from the Department of Chemistry, Northwestern University, 2145 Sheridan Road, Evanston, Illinois 60208-3113

Received October 27, 1999

Abstract: A study aimed at understanding the factors that control the optical properties of DNA-linked gold nanoparticle aggregates containing oligonucleotide linkers of varying length (24−72 base pairs) is described. In this system, ∼15 nm diameter Au particles modified with (alkanethiol)-12 base oligomers are hybridized to a series of oligonucleotide linkers ranging from 24 to 72 base pairs (∼80−240 Å) in length. Aggregated at room temperature, the various macroscopic nanoparticle assemblies have plasmon frequency changes that are inversely dependent on the oligonucleotide linker length. Upon annealing at temperatures close to the melting temperature of the DNA, the optical properties of the DNA-linked assemblies containing the longer linkers (48 and 72 base pairs) red-shift until they are similar to the assemblies containing the shorter linkers (24 base pairs). The pre- and postannealed DNA-linked assemblies were characterized by sedimentation rate, transmission electron microscopy, dynamic light scattering, and UV−vis spectroscopy which show that the oligonucleotide linker length kinetically controls the size of the aggregates that are formed under the preannealed conditions, thereby controlling the optical properties. Through the use of small-angle X-ray scattering and electrodynamic modeling in conjunction with the techniques mentioned above, we have determined that the temperature-dependent optical changes observed upon annealing of the aggregates containing the longer oligonucleotides (48 and 72 base pairs) can be attributed to aggregate growth through an "Ostwald ripening" mechanism (where larger aggregates grow at the expense of smaller aggregates). This type of aggregate growth leads to the red-shift in plasmon frequency observed for the aggregates. Significantly, these experiments provide evidence that the optical properties of these DNA-linked nanoparticle assemblies are governed by aggregate size, regardless of oligonucleotide linker length, which has important implications for the development of colorimetric detection methods based on these nanoparticle materials.

Introduction

Recently, we reported a new "programmed assembly" strategy[1] for organizing nanoparticles into periodic functional materials.[2−4] This strategy utilizes nanoparticle building blocks modified with alkanethiol-capped oligonucleotides (single-stranded DNA) and complementary linker oligonucleotide (DNA) strands to form extended structures with control over particle chemical composition, periodicity, and aggregate thermal stability, thereby providing control over the optical, mechanical, and electrical properties of these hybrid bioinorganic materials.[5] Importantly, we already have exploited the optical properties of one such system, formed from 13 to 17 nm diameter Au particles, in the development of a highly selective colorimetric diagnostic method for DNA.[6] This diagnostic method relies on the distance-dependent optical properties of gold particles.[7] Specifically, it is well documented that the plasmon frequency of a collection of gold particles can be controlled by adjusting the distance between discrete nanoparticles or layers of nanoparticles.[8] Based on these studies, we

* To whom correspondence should be addressed. E-mail: camirkin@chem.nwu.edu; r-letsinger@chem.nwu.edu; and schatz@chem.nwu.edu.

‡ Department of Chemistry and Center for Nanofabrication and Molecular Self-Assembly.

† Department of Chemistry and of Biochemistry, Molecular Biology, and Cell Biology.

(1) Mirkin, C. A.; Letsinger, R. L.; Mucic, R. C.; Storhoff, J. J. *Nature* **1996**, *382*, 607−609.

(2) For other solution-based methods, see: (a) Alivisatos, A. P.; Johnsson, K. P.; Peng, X.; Wilson, T. E.; Loweth, C. J.; Bruchez, M. P., Jr.; Schultz, P. G. *Nature* **1996**, *382*, 609−611. (b) Cusack, L.; Rizza, R.; Gorelov, A.; Fitzmaurice, D. *Angew. Chem., Int. Ed. Engl.* **1997**, *36*, 848−851. (c) Niemeyer, C. M.; Burger, W.; Peplies, J. *Angew. Chem., Int. Ed. Engl.* **1998**, *37*, 2265−2268. (d) Sastry, M.; Lala, N.; Patil, V.; Chavan, S. P.; Chittiboyana, A. G. *Langmuir* **1998**, *14*, 4138−4142. (e) Shenton, W.; Davis, S. A.; Mann, S. *Adv. Mater.* **1999**, *11*, 449−452. (f) Liu, J.; Mendoza, S.; Roman, E.; Lynn, M. J.; Xu, R.; Kaifer, A. E. *J. Am. Chem. Soc.* **1999**, *121*, 4304−4305.

(3) For template-based methods, see: (a) Coffer, J. L.; Bigham, S. R.; Li, X.; Pinizzotto, R. F.; Rho, Y. G.; Pirtle, R. M.; Pirtle, I. L. *Appl. Phys. Lett.* **1996**, *69*, 3851−3853. (b) Shenton, W.; Pum, D.; Sleytr, U. B.; Mann, S. *Nature* **1997**, *466*, 585−587. (c) Bekele, H.; Fendler, J. H.; Kelly, J. W. *J. Am. Chem. Soc.* **1999**, *121*, 7266−7267.

(4) For recent reviews, see: (a) Storhoff, J. J.; Mucic, R. C.; Mirkin, C. A. *J. Cluster Sci.* **1997**, *8*, 179−216. (b) Storhoff, J. J.; Mirkin, C. A. *Chem. Rev.* **1999**, *99*, 1849−1862.

(5) (a) Mucic, R. C.; Storhoff, J. J.; Mirkin, C. A.; Letsinger, R. L. *J. Am. Chem. Soc.* **1998**, *120*, 12674−12675. (b) Mitchell, G. P.; Mirkin, C. A.; Letsinger, R. L. *J. Am. Chem. Soc.* **1999**, *121*, 8122−8123.

(6) (a) Elghanian, R.; Storhoff, J. J.; Mucic, R. C.; Letsinger, R. L.; Mirkin, C. A. *Science* **1997**, *277*, 1078−1081. (b) Storhoff, J. J.; Elghanian, R.; Mucic, R. C.; Mirkin, C. A.; Letsinger, R. L. *J. Am. Chem. Soc.* **1998**, *120*, 1959−1964.

(7) (a) Brust, M.; Bethell, D.; Schiffrin, D. J.; Kiely, C. *Adv. Mater.* **1995**, *7*, 795−797. (b) Freeman, R. G.; Grabar, K. C.; Allison, K. J.; Bright, R. M.; Davis, J. A.; Guthrie, A. P.; Hommer, M. B.; Jackson, M. A.; Smith, P. C.; Walter, D. G.; Natan, M. J. *Science* **1995**, *267*, 1629−1632. (c) Heath, J. R.; Knobler, C. M.; Leff, D. V. *J. Phys. Chem. B* **1997**, *101*, 189−197. (d) Pileni, M. *New J. Chem.* **1998**, 693−702. (e) Lin, X. M.; Wang, G. M.; Sorensen, C. M.; Klabunde, K. J. *J. Phys. Chem. B* **1999**, *103*, 5488−5492.

(8) (a) Schmitt, J.; Decher, G.; Dressick, W. J.; Brandow, S. L.; Geer, R. E.; Shashidar, R.; Calvert, J. M. *Adv. Mater.* **1997**, *9*, 61−65. (b) Collier, C. P.; Saykally, R. J.; Shiang, J. J.; Henrichs, S. E.; Heath, J. R. *Science* **1997**, *277*, 1978−1981.

10.1021/ja993825l CCC: $19.00
Published on Web 04/25/2000

Scheme 1

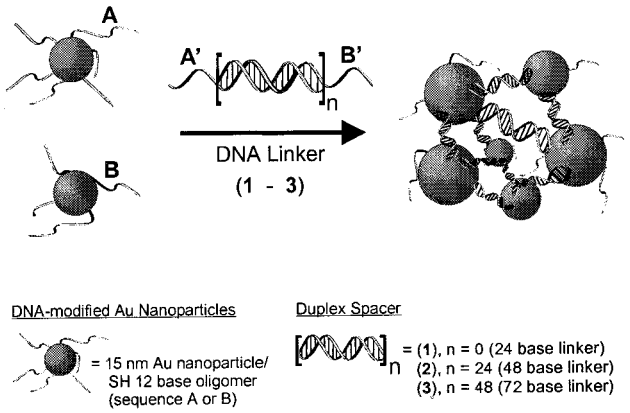

rationalized that it might be possible to control the optical properties of our composite materials by controlling the length of the DNA linker molecules/target molecules and the average distance between the particles, Scheme 1. Moreover, this system poses an unprecedented opportunity to explore this relationship over a length scale that is broader and longer than the length scale associated with conventional organic interconnect molecules. Stable oligonucleotide interconnects, in the 8 to 200 nucleotide range (~27−680 Å), can be readily synthesized via standard solid-phase procedures.[9]

Early solution and modeling studies on the optical properties of metal nanoparticle aggregates and agglomerates focused on relatively small structures (2−100 particles) with very small nanoparticle spacings (≅0).[10] The general conclusions from these studies are that for closely spaced metal nanoparticles, only small collections (2−10) of particles are required to give substantial shifts in the plasmon resonance. Our DNA-based assembly method results in macroscopic assemblies consisting of thousands of particles and, therefore, offers a unique opportunity to study the collective properties of large nanoparticle network assemblies that have longer interparticle distances than previously studied systems. Herein, we show that tailorability of the optical properties using this programmed assembly approach is indeed achievable through the use of different length DNA particle interconnects, but the observed optical effects in this system are as much a function of aggregate size (which is under kinetic control; growth rate is dependent upon linker length) as interparticle distance. This surprising result is significant since it impacts not only our understanding of the colorimetric response associated with our diagnostic method but also any effort aimed at using this approach to tailor the optical properties of these novel network materials.

Experimental Section

Reagents. $HAuCl_4 \cdot 3H_2O$ and trisodium citrate were purchased from Aldrich chemical company. All DNA synthesis reagents were purchased from Glen Research, Sterling, VA. NAP-5 columns (Sephadex G-25 Medium, DNA grade) were purchased from Pharmacia Biotech (Uppsala, Sweden).

Instrumentation. Electronic absorption spectra and melting analyses were recorded using a HP 8453 diode array spectrophotometer equipped with a HP89090a Peltier Temperature Controller. High Performance Liquid Chromatography (HPLC) was performed with a HP series 1100 HPLC. Transmission Electron Microscopy (TEM) images were recorded with a Hitachi 8100 TEM. An Eppendorf 5415C centrifuge was used for centrifugation of Au nanoparticle solutions. Nanopure H_2O (18.1 MΩ) purified with a Barnstead NANOpure ultrapure water system was used for all experiments.

Preparation of 3′ or 5′-(Alkanethiol)oligonucleotide-Modified Au Nanoparticles. The methods for preparing 13−17 nm diameter Au particles,[11] 3′ or 5′ alkanethiol-capped oligonucleotides, and (alkanethiol)oligonucleotide-modified Au nanoparticles (referred to as DNA-modified Au particles) were reported previously.[6b] The gold particles prepared by the citrate method in this size range are reasonably monodisperse (typically ≤15% standard deviation) but vary in average size for different preparations (typically 13−17 nm in diameter). The gold nanoparticles used in this study have an average diameter of 15.4 nm as measured by TEM. The extinction coefficient for the plasmon band at 520 nm was previously determined to be $\epsilon_{520} \approx 2.40 \times 10^8$ M^{-1} cm^{-1}.[5a] The concentrations of the DNA-modified Au nanoparticle solutions were determined using the absorbance values at 520 nm in conjunction with the extinction coefficient. The sequences of the 3′ and 5′ alkanethiol-capped 12 base oligonucleotides used in this study are as follows

5′ SH-$(CH_2)_6$-CGC-ATT-CAG-GAT (sequence **A** in scheme 1)

3′ SH-$(CH_2)_3$-ATG-CTC-AAC-TCT (sequence **B** in scheme 1)

Preparation and Characterization of Linker DNA. Oligonucleotides under 50 bases in length were synthesized on a 1 μmol scale with a Milligene Expedite DNA synthesizer via standard phosphoramidite chemistry.[9] The 72 base oligonucleotide was synthesized using 1000 Å CPG solid support on a 0.2 μmol scale. The oligonucleotides were purified using standard HPLC procedures that were reported previously.[6b] The final concentration of the oligonucleotides were determined by the magnitude of the absorbance at 260 nm, and the extinction coefficient at 260 nm calculated using a formula based on nearest neighbors.[12] The sequences of the DNA linkers are shown in Chart 1. Both the 48 base and 72 base linkers are double-stranded oligonucleotides that contain 12 base single-stranded "sticky ends" that are complementary to the oligonucleotides attached to the gold nanoparticles. The 24 base linker consists of one single-stranded oligonucleotide.

Melting analyses of the DNA linkers were performed by monitoring the absorbance at 260 nm at 1 min intervals, with a holding time of 1 min/deg. T_m values were calculated from the first derivative of the change in extinction at 260 nm. Reported T_m values were rounded to the nearest degree. Melting analyses of 0.78 μM solutions of the 48 base (**2**) and 72 base (**3**) linkers were recorded in 0.3 M NaCl, 10 mM phosphate (pH 7) hybridization buffer (referred to as 0.3 M PBS) yielding T_m values of 70 and 81 °C, respectively. The melting analyses of the 24 (**1**), 48 (**2**), and 72 (**3**) base linkers with the complementary 12 base oligonucleotides (sequences **A** and **B** shown above, without thiol modification) were evaluated to ensure the binding characteristics of the DNA linkers. All three melting analyses were performed at a final DNA concentration of 1.56 μM in 0.3 M PBS hybridization buffer. The 24 base linker (**1**) with complementary 12 base oligonucleotides (**A** and **B**) exhibited a typical single melting transition with a T_m value of 54 °C.[6b] The 48 base linker (**2**) with complementary 12 base oligonucleotides (**A** and **B**) exhibited two discrete melting transitions at the appropriate temperatures: the first transition, which is due to the melting of the 12 base oligonucleotide ends, occurs at a T_m of 55 °C, while a second transition due to the melting of the 24 base interior portion of the DNA occurs at 72 °C. The 72 base linker (**3**) with complementary 12 base oligonucleotides (**A** and **B**) also exhibited two discrete melting transitions at the appropriate temperatures: the first transition, which is due to the melting of the 12 base oligonucleotide ends, occurs at a T_m of 55 °C, while a second transition due to the melting of the 48 base interior portion of the DNA occurs at 81 °C.

Ten μM DNA linker stock solutions were prepared in 0.3 M PBS hybridization buffer. For the longer DNA linkers (**2** and **3**), the solutions

(9) Eckstein, F. *Oligonucleotides and Analogues*, 1st ed.; Oxford University Press: New York, 1991.

(10) (a) Quinten, M.; Kreibig, U. *Surf. Sci.* **1986**, *172*, 557−577. (b) Schonauer, D.; Quinten, M.; Kreibig, U. *Z. Phys. D* **1989**, *12*, 527−532. (c) Yang, W.-H.; Schatz, G. C.; Van Duyne, R. P. *J. Chem. Phys.* **1995**, *103*, 869−875.

(11) (a) Grabar, K. C.; Freeman, R. G.; Hommer, M. B.; Natan, M. J. *Anal. Chem.* **1995**, *67*, 735−743. (b) Frens, G. *Nat. Phys. Sci.* **1973**, *241*, 20−22.

(12) Fasman, G. *Handbook of Biochemistry and Molecular Biology*, 3rd ed.; CRC Press: Cleveland, OH, 1975.

Chart 1

24 base linker (**1**) :

5' TAC GAG TTG AGA ATC CTG AAT GCG 3'

48 base linker (**2**):

5' TAC GAG TTG AGA CCG TTA AGA CGA GGC AAT CAT GCA ATC CTG AAT GCG 3'
3'GGC AAT TCT GCT CCG TTA GTA CGT 5'

72 base linker (**3**):

5' TAC GAG TTG AGA CCG TTA AGA CGA GGC AAT CAT GCA TAT ATT GGA CGC TTT ACG GAC AAC ATC CTG AAT GCG 3'
3' GGC AAT TCT GCT CCG TTA GTA CGT ATA TAA CCT GCG AAA TGC CTG TTG 5'

Scheme 2

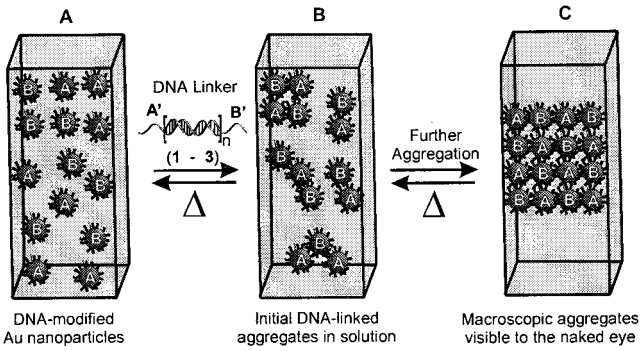

were annealed at 80 °C for 10 min to remove kinetic structures, followed by standing at room temperature for 1 h. These stock solutions were used for all of the studies reported herein.

Preparation and Characterization of DNA-Linked Au Nanoparticle Aggregates. For the DNA-linked Au nanoparticle solutions, 6 μL of the appropriate 10 μM DNA linker solution (**1**−**3,** see Scheme 1) was added to a 2.7 nM solution (994 μL) of DNA-modified Au nanoparticles (1:1 mixture of **A** and **B** in Scheme 2) in 0.3 M PBS hybridization buffer. The final spectra in Figure 3A were recorded after the samples had fully precipitated and were subsequently resuspended. Annealing experiments were performed by heating the DNA-linked aggregates (**1**−**3**, numbered according to DNA linker added) with sample agitation to 48 °C in a glass cuvette for 2 h while monitoring the UV−visible spectrum. Melting analyses were performed by monitoring the UV−visible signature of the aggregates at 1 min intervals, as the temperature was increased from 25 to 75 °C with a holding time of 1 min/deg, with agitation to maintain homogeneity. T_m values were calculated from the first derivative of the change in extinction at 700 nm, which is highly sensitive to aggregate dissociation.[6b] Reported T_m values were rounded to the nearest degree.

Dynamic Light Scattering. DLS measurements were performed using a Brookhaven Instruments Corporation model BI-9000AT digital autocorrelator and photon counter with a model BI-200SM goniometer. Incident light was provided by an argon ion laser (λ_{ex} = 514.5 nm) operating at 300 mW (Lexel Corp). Scattered light was collected at a fixed angle of 90°. The DNA-modified gold nanoparticles were filtered through a 0.22 μm acetate membrane filter prior to mixing to remove any dust particles. The DNA-linked Au nanoparticle aggregate samples were prepared as described above.

Transmission Electron Microscopy. TEM samples were prepared by dropping two 10 μL aliquots of the aggregate solutions onto a holey carbon coated copper grid. After deposition, any remaining solution was wicked away, and the grids were dried for 30 min under ambient conditions. The aggregates were imaged using a Hitachi 8100 Transmission Electron Microscope operating at 200 keV.

Small-Angle X-ray Scattering (SAXS). The SAXS experiments were performed at Argonne National Laboratories using the Dupont-Northwestern-Dow Collaborative Access Team (DND-CAT) Synchrotron Research Center located at Sector 5 of the Advanced Photon Source. The DNA-linked aggregates and DNA-modified Au particles were analyzed using 1.54 Å radiation, and scattered photons were collected on a CCD detector. Experimental data were corrected for background scattering and sample absorption. The scattering vector s (nm^{-1}), which is inversely proportional to the characteristic d spacing, is defined as $s = 2\sin(\theta)/\lambda$, where 2θ is the scattering angle and λ is the wavelength of the incident radiation. The scattering intensity $I(s)$ of the DNA-linked aggregates is proportional to the static structure factor $S(s)$ as follows: $I(s) = F^2(s)\cdot S(s)$,[13] where $F^2(s)$ is the scattering intensity associated with the dispersed DNA-modified particles without linker, and the particles are taken to be monodisperse.

Calculations of UV−vis Extinction Spectra

Mie theory[14] was used to calculate extinction spectra for the DNA-linked nanoparticle aggregates from the dielectric functions of the aggregates. The aggregate dielectric functions were derived from the dielectric functions of the nanoparticles and of the aqueous medium using a recently developed effective medium theory.[15] The theory is a refinement of Maxwell−Garnett theory that accounts for the dynamical nature of the interaction of light with the nanoparticles and of the particle−particle interactions. This theory matches well with the results of explicit particle (coupled-dipole and coupled-multipole) calculations for the DNA-linked gold nanoparticle aggregates of interest to this study.[15] The values of the gold dielectric functions were taken from refs 16 and 17 as described in ref 18a and corrected for quantum confinement[18b] of the metal free electrons due to the small size (15.4 nm) of the Au particles. The dielectric constant of the medium was taken to be 1.33. Small variations of the dielectric constant of the medium immediately outside the particles due to the presence of the DNA layer were ignored based on experimental data (vide infra).

Results and Discussion

DNA-Linked Au Nanoparticle Assemblies from 24, 48, and 72 Base Pair Linkers. Our approach to investigating the effects of DNA linker length on Au nanoparticle aggregate formation is outlined in Scheme 1. First, two batches of Au particles (15.4 nm average diameter) are chemically modified with alkanethiol-capped 12 base DNA strands (**A** and **B**) using a procedure reported previously.[6b] The DNA-modified Au nanoparticles are stored at 0.3 M PBS, 0.01% azide prior to use. These conditions were chosen because they are compatible with the modified particles and are conducive to rapid DNA

(13) Glatter, O.; Kratky, O. *Small-Angle X-ray Scattering*; Academic: New York, 1982.
(14) Bohren, C. F.; Huffman, D. R. *Absorption and Scattering of Light by Small Particles*; Wiley: New York, 1983; p 101.
(15) (a) Lazarides, A. A.; Schatz, G. C. J. Chem. Phys. Submitted for publication. (b) Lazarides, A. A.; Kelly, K. L.; Jenson, T. R.; Schatz, G. C. *Theo. Chim.* **2000**, in press.
(16) Johnson, P. B.; Christy, R. W. *Phys. Rev. B* **1972**, *6*, 4372.
(17) Theye, M.-L. *Phys. Rev. B* **1972**, *2*, 4370.
(18) (a) Lazarides, A. A.; Schatz, G. C. *J. Phys. Chem. B* **2000**, *104 (6)*, 460−467. (b) Kraus, W. A.; Schatz, G. C. *J. Chem. Phys.* **1983**, *79*, 6130−6139.

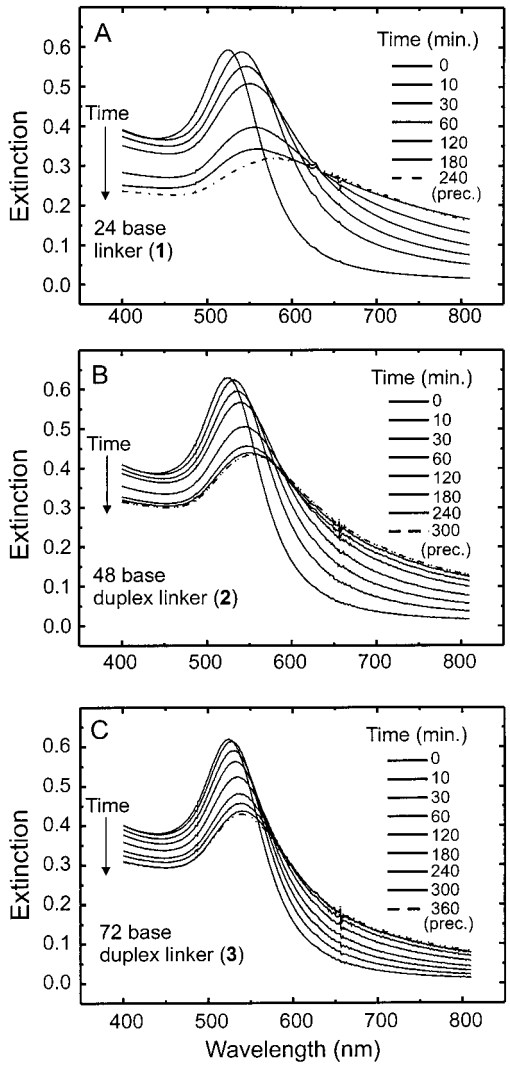

Figure 1. Changes in extinction as a function of time in the visible region of the UV−visible spectra for nanoparticle aggregates grown from DNA linkers **1**−**3**. The *y*-axes are labeled as "extinction" since the larger aggregate structures will contain scattering as well as absorbance components.

hybridization and particle aggregation when the particles are introduced to complementary DNA linkers.[6b] The DNA-modified Au nanoparticle solutions are dark red in color, with a plasmon band centered at 524 nm. DNA linker sequences were designed to have 12 base "sticky ends" (**A′** and **B′**) that are complementary to the DNA attached to the nanoparticles (**A** and **B**) and a variable "duplex spacer" portion of 0, 24, or 48 bases (DNA linkers **1**−**3**, respectively) to control the DNA linker length and particle spacing, Scheme 1.

Initial experiments were performed by adding a DNA linker (**1**−**3**, final DNA concentration = 0.06 μM) to a solution of DNA-modified Au nanoparticles **A** and **B** (1:1 ratio, final nanoparticle concentration = 2.7 nM) at 25 °C, Scheme 2. This was done for each of the different length DNA linkers, **1**−**3**. In these experiments, the solutions were agitated before optical spectra were recorded to ensure homogeneity of the particle suspension. The formation of DNA-linked Au nanoparticle aggregates (**1**−**3**, numbered according to DNA linker added) was followed by monitoring the surface plasmon band in the UV−visible spectrum as a function of time, Figure 1A−C. In each case, the surface plasmon band gradually red-shifted from 524 nm as aggregate growth occurred through DNA hybridization,[1] and eventually macroscopic aggregates visible to the naked eye were observed in solution, Scheme 2 and Figure 1A−C. Significant differences in the optical spectra were observed during the formation of the aggregates containing the different length DNA linkers (**1**−**3**). First, the rate of change of the surface plasmon band (breadth and maximum) was inversely dependent on the length of the DNA linker, with the 24 base linker system (shortest linker) exhibiting the largest changes at the fastest rate. The plasmon band maximum stopped changing under these conditions after 3, 4, and 5 h for the 24, 48, and 72 base linked aggregates, respectively. For this set of experiments, the macroscopic DNA-linked aggregates (**1**−**3**) exhibited final plasmon band shifts at λ_{max} = 581 (**1**), 550 (**2**), and 540 (**3**) nm, where the magnitude of the plasmon frequency change from 524 nm was inversely dependent upon linker length, Figure 1A−C and Table 1. For the 72 base linked aggregate (**3**), the precipitate had a reddish color that was easily distinguishable from the intermediate reddish-purple and deeper purple precipitates formed using the 48 base (**2**) and 24 base (**1**) linkers, respectively. In previous studies, we have monitored UV (260 nm) and longer wavelength (650−700 nm) nanoparticle signatures that are very sensitive to aggregate formation and dissociation.[6b] In the study reported herein, we observed significant extinction differences in these spectral regions for the aggregates containing the different length DNA linkers (**1**−**3**), Table 1. Therefore, the length of the DNA (estimated at 82, 164, and 246 Å for linkers **1**−**3**, respectively, based on B-form DNA) used to link the particles provides one level of control over the optical properties of the aggregates formed from the respective linkers under the stated conditions.

Melting Analyses. A "melting analysis" was performed on each of the DNA-linked aggregates (**1**−**3**) to verify DNA hybridization and the reversibility of aggregate formation (see the Experimental Section for details). In these experiments, the nanoparticle signature at 700 nm was monitored as a function of temperature. As discussed in previous studies,[1] a sharp decrease in extinction at 700 nm was observed when the DNA-linked nanoparticle aggregates (**1**−**3**) dissociate, Figure 2A. The melting temperatures (T_m) for DNA-linked aggregates **1**−**3** were 54, 54, and 56 °C, respectively, Table 1. These values are consistent with aggregate dissociation driven by the dehybridization of the short "sticky ends" of the DNA linkers from the DNA-modified nanoparticles. The T_m values of the longer duplex linker spacers (**2** and **3**, see Scheme 1) are significantly higher (see the Experimental Section) than the T_m values for the short "sticky ends" and, therefore, do not contribute significantly to the melting profiles reported herein. Although the melting temperatures of the DNA-linked aggregates are similar, a noteworthy increase in extinction at 700 nm was observed prior to aggregate dissociation for the aggregates containing the 48 and 72 base linkers (**2** and **3**). The temperature range of this extinction increase at 700 nm was approximately 37−50 °C (shaded box), Figure 2A. Additionally, the 48 base and 72 base linked aggregates exhibited significant plasmon band red shifts, broadening, and a significant drop in intensity at the extinction maximum in this same temperature region as a function of time, Scheme 3 and Figure 2B. These major extinction and plasmon band changes in the 400 to 800 nm region of the spectrum occur in a direction opposite of that normally observed for aggregate dissociation.[6b] Similar optical transformations were not observed for the 24 base linked aggregate (**1**) upon annealing. These data indicate that a major structural change is thermally initiated prior to aggregate dissociation for the 48 base and 72 base linked aggregates (**2** and **3**).

Table 1. Physical Properties of DNA-Linked Au Nanoparticle Aggregates before and after Annealing

	before annealing						after annealing					
DNA linker	λ_{max} (nm)	ext.[a] at λ_{max} (AU)	ext. at 260 nm (AU)	ext. at 700 nm (AU)	S^b (min)	T_m (°C)	λ_{max} (nm)	ext.[a] at λ_{max} (AU)	ext. at 260 nm (AU)	ext. at 700 nm (AU)	S^b (min)	T_m (°C)
1	581	0.32	0.26	0.23	33	54	579	0.32	0.28	0.24	31	54
2	550	0.43	0.39	0.20	65	54	576	0.34	0.32	0.24	32	55
3	540	0.44	0.44	0.14	106	56	571	0.33	0.33	0.23	35	55

[a] Ext. = extinction. [b] *S* for sedimentation is defined in the text in the Results and Discussion section.

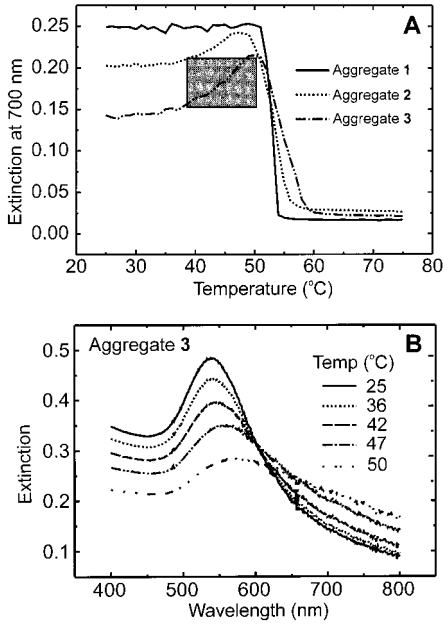

Figure 2. (A) Thermal dissociation curves for each of the macroscopic aggregates containing the different length DNA linkers **1**−**3**. The extinction at 700 nm was monitored as a function of temperature for each of the aggregates. (B) Changes in the visible spectrum of the 72 base linked aggregate (**3**) over the temperature range designated by the shaded box in Figure 2A.

Scheme 3

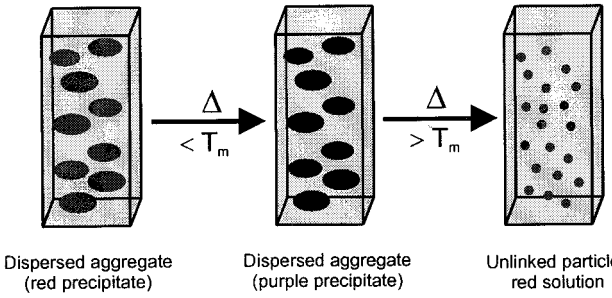

Annealing Studies of the 24, 48, and 72 Base Linked Aggregates. To further investigate this unusual temperature-dependent optical phenomenon, each of the macroscopic DNA-linked aggregates (**1**−**3**) formed at room temperature was heated just below the aggregate melting temperature (48 °C) for 2 h while monitoring the changes in the surface plasmon band. As expected, plasmon frequency red shifts and extinction changes (monitored at the extinction maximum, 260 nm, and 700 nm) were observed for the 48 and 72 base linked aggregates (**2** and **3**) during the first 30 min of the annealing process, while very little change was observed in the spectrum of the 24 base linked aggregates (**1**). After annealing all three aggregate solutions for a period of 2 h, the optical spectra of the 48 and 72 base linked aggregates (**2** and **3**) were nearly identical with the optical spectrum of the 24 base linked aggregates (**1**), Figure 3 and

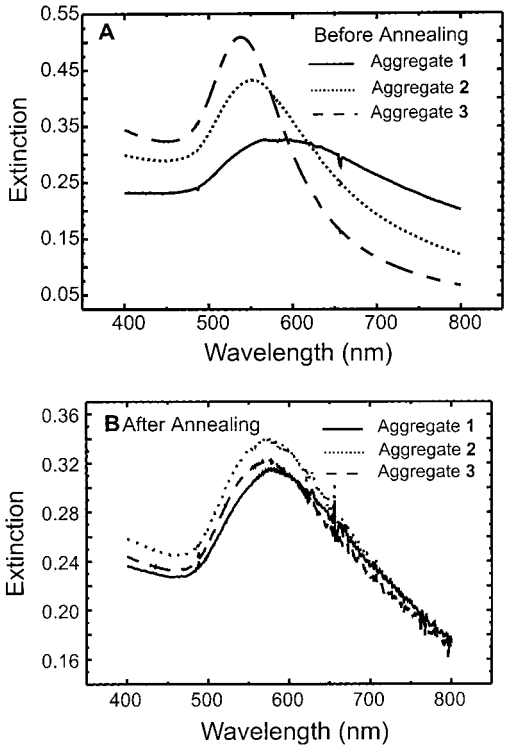

Figure 3. (A) Optical spectra for the preannealed DNA-linked aggregates **1**−**3**. (B) Optical spectra for postannealed DNA-linked aggregates **1**−**3**.

Table 1. Accordingly, each solution of DNA-linked aggregates (**1**−**3**) was purple after aggregate annealing, regardless of linker length. This suggests that the 48 and 72 base linked aggregates (**2** and **3**) form kinetically stable structures under the preannealing conditions; these structures can be thermally transformed into thermodynamic aggregate products upon annealing. These data also raise the question of what controls the optical properties of DNA-linked Au nanoparticle aggregates? Two possible explanations for the optical changes observed upon annealing are a change in DNA conformation, which leads to a change in interparticle distance, or an increase in the number of particles that comprise the aggregates (e.g. aggregate size). Further analysis was required to answer this extremely important fundamental question (vide infra).

The melting analyses of each of the annealed DNA-linked aggregates (**1**−**3**) show that complete aggregate dissociation occurs as evidenced by a return to the original extinction values associated with the dispersed particles. This result indicates that the particles do not fuse together during the annealing or melting processes, a result which has been independently confirmed by TEM analysis of the samples (vide infra). In addition, the melting temperatures and observed extinction changes were nearly identical for the annealed aggregates (**1**−**3**), Table 1. To confirm that the optical changes observed upon annealing were due to the DNA-linked aggregate structures and not excess DNA or excess Au particles in solution, the supernatant of the 72

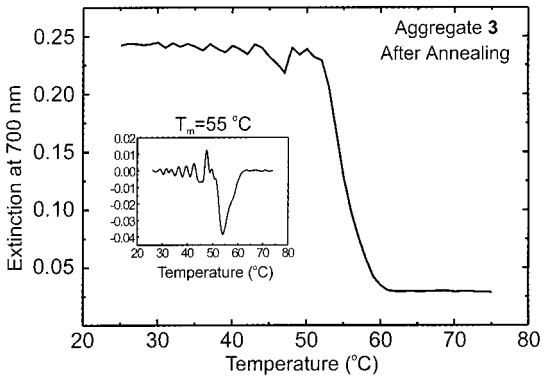

Figure 4. Thermal dissociation curve for the solution containing the annealed 72 base linked aggregates **3**. The temperature was recorded in 1 °C increments with a holding time of 1 min/deg while monitoring the extinction at 700 nm. The inset shows the derivative curve of the melting analysis.

base linked aggregate (**3**) was removed, and the precipitated aggregates were washed and subsequently redispersed in fresh buffer (0.3 M PBS). The supernatant showed very minimal absorption for both the plasmon region (Abs_{520} = 0.028 AU, ≤5% of solution added) and the region at 260 nm (Abs_{260} = 0.053 AU, mainly due to nanoparticle absorbance in this region[6b]), indicating that minimal individual nanoparticles and linker DNA were left in solution after aggregate formation. Moreover, the 72 base linked aggregate (**3**) dispersed in fresh buffer exhibited optical changes upon annealing and aggregate dissociation properties that were nearly identical with the same aggregate that had not been redispersed in fresh buffer. Finally, the annealed structures, unlike the preannealed structures, do not show a rise in extinction at 700 nm prior to aggregate dissociation. Instead, they show a characteristic sharp melting transition (the annealed 72 base linked aggregate **3** is shown as a representative example), Figure 4.

It also was necessary to confirm that the optical properties of the gold nanoparticles do not change significantly upon DNA binding or hybridization since the state and structure of the DNA could potentially affect the local dielectric medium, which might contribute to the significant surface plasmon band shifts observed during both aggregation and annealing.[19] We previously reported that derivatizing citrate modified gold nanoparticles with alkanethiol-12 base oligonucleotides, which are subsequently dispersed in 0.3 M PBS, leads to only a small shift in the surface plasmon band from 519 to 524 nm, which may be in part due to a change in the dielectric medium associated with both DNA and buffer.[6b] More importantly, we have prepared a solution containing the 72 base DNA linker and one of the complementary DNA-modified gold nanoparticles (either sequence **A** or sequence **B**, but not both in solution to prevent particle aggregation) under the same experimental conditions as the aggregate solutions (vide supra) and monitored it spectroscopically (UV−vis) during hybridization and melting. This experiment was designed to determine if the hybridization and melting of linker DNA to the DNA-modified gold nanoparticle surface, *without gold nanoparticle aggregation*, would result in any significant changes in the surface plasmon band. No significant surface plasmon band changes were observed for the 72 base linker/DNA-modified gold nanoparticle solutions after addition of the linker or during the melting analysis. Therefore, DNA hybridization and melting at the gold nanoparticle surface do not significantly affect the optical properties and cannot account for the surface plasmon band changes associated with gold nanoparticle aggregation or annealing.

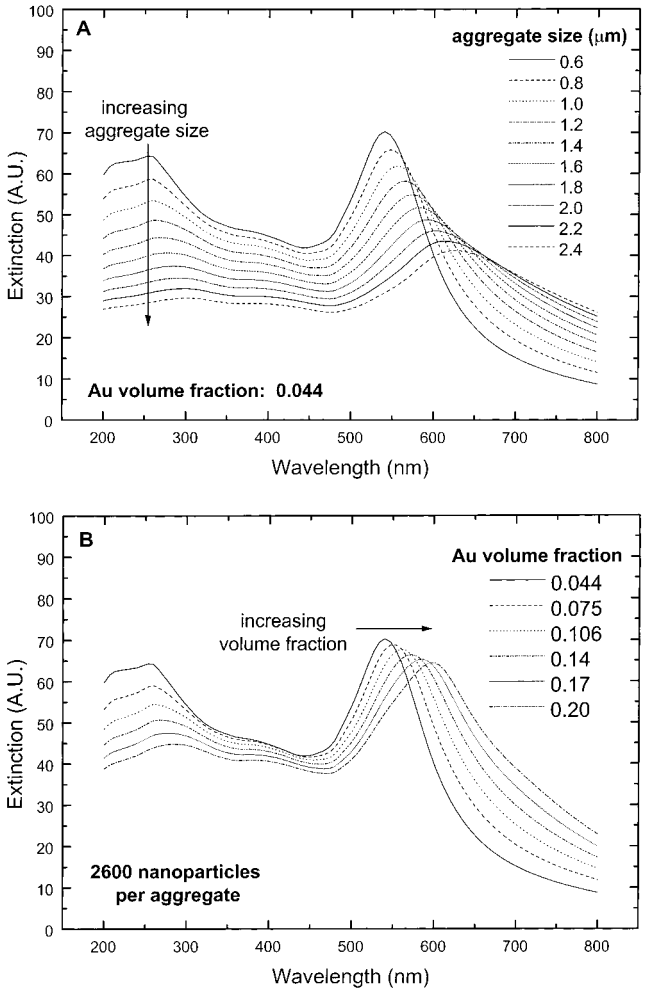

Figure 5. Electrodynamic modeling calculations for the 72 base linked aggregates (**3**). (A) Changes in UV−vis extinction spectra as the aggregate size changes with constant gold volume fraction. (B) Changes in UV−vis extinction spectra as the gold volume fraction changes, with the number of particles per aggregate at a fixed value.

Theoretical Studies of the Dependence of the UV−Vis Spectra upon Aggregate Size and Volume Fraction. To clarify the structural basis for the optical phenomenon associated with annealing, simulations of the UV−vis spectra were performed for the 72 base linked aggregates by changing interparticle distance (metal volume fraction) or aggregate size. It is important to note that previous simulations have demonstrated that the optical spectra are insensitive to the aggregate microstructure (e.g. FCC, BCC).[18a] However, for purposes of calculating metal volume fraction, a linker length of 230 Å and a BCC structure were assumed. A metal volume fraction of 0.044 was calculated based on these parameters and the aggregate size was determined by fitting the calculated spectrum to the preannealed experimental spectrum. The resulting theoretical spectrum for a 600 nm aggregate is shown in Figure 5A; the peak in the extinction at 540 nm matches the experimentally measured plasmon peak as listed in Table 1. Additional calculations were performed for aggregates either larger or denser. Extinction spectra for a series of larger aggregates are also included in Figure 5A. As the aggregate size increases (without decreasing interparticle distance), the plasmon band red shifts and broadens significantly, thereby reducing the peak extinction. Extinction spectra for aggregates

(19) Jensen, T. R.; Duval, M. L.; Kelly, L.; Lazarides, A. A.; Schatz, G. C.; Van Duyne, R. P. *J. Phys. Chem. B* **1999**, *103*, 9846−9853.

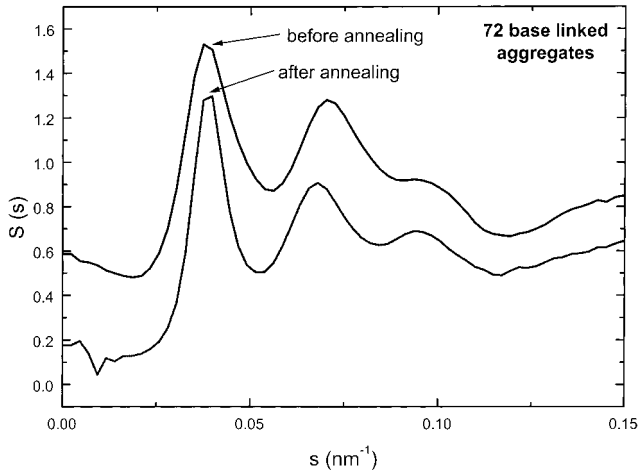

Figure 6. SAXS of the 72 base linked aggregates (**3**) before and after annealing. Arrows are used to highlight the location of the first-order diffraction peak before and after annealing.

composed of equal numbers of particles but with various smaller separations between particles are illustrated in Figure 5B. Densification appears to red shift the plasmon peak without causing significant loss in peak extinction. The experimentally observed signature of annealing for the 72 base linked aggregates (see Figure 2B) is a red shifting of the plasmon band accompanied by a significant reduction and broadening in the extinction. The simulations indicate that the experimentally observed optical changes associated with annealing are much more consistent with a change in aggregate size than a change in volume fraction. Furthermore, as illustrated in ref 15, an increase in the gold volume fraction by a factor of 2 yields only a few percent drop in the peak extinction of the 72 base linked aggregates. Thus, while the optical spectra alone do not rule out the possibility of some densification of the 72 base linked aggregates upon annealing, a factor of 5 increase in the gold volume fraction would be required to explain the observed spectral changes without a simultaneous increase in aggregate size. SAXS measurements in conjunction with sedimentation rate, DLS, and TEM were performed to confirm the theoretical conclusions regarding the structural effects of annealing (vide supra).

Small-Angle X-ray Scattering (SAXS). To experimentally investigate whether interparticle distance changes occur upon annealing, the 72 base linked aggregates (**3**) were analyzed by SAXS since the largest optical shifts were observed with this system. Figure 6 shows the static structure factor $S(s)$ for the 72 base linked aggregates before and after annealing. Importantly, the first-order diffraction peak ($s = 0.038$ nm^{-1}, highlighted by an arrow) of the 72 base linked aggregates, which is an indicator of the center-to-center nanoparticle distance, does not shift upon annealing and exhibits only a small increase in sharpness. This indicates that the interparticle distance of these DNA-linked aggregates (**3**) does not change significantly upon annealing. Additionally, these data rule out a total collapse of the aggregates resulting in large changes in volume fraction, which according to the electrodynamic modeling would be required to produce the extinction drop that is experimentally observed in this system. It is important to note that large shifts in the first-order diffraction peak of these aggregates associated with drying have been observed (s shifts from 0.038 to 0.086 nm^{-1} upon drying), which indicates that this peak is sensitive

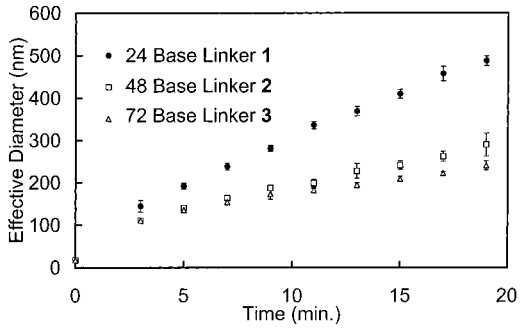

Figure 7. Change in the effective diameter as a function of time for nanoparticle aggregates grown from DNA linkers **1**−**3**, as measured by dynamic light scattering. The scattering data were collected over 30 s time periods at 2 min intervals as nanoparticle aggregation occurred. The error bars represent the standard deviation for a series of three measurements.

Scheme 4

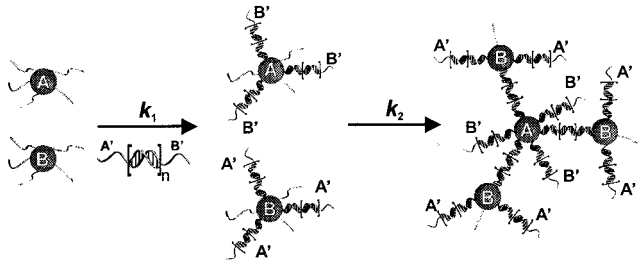

to changes in interparticle distance.[20] On the basis of these data, we rationalized that the optical changes associated with annealing of the DNA-linked aggregates must be governed by factors other than interparticle distance.

Dynamic Light Scattering (DLS) of DNA-Linked Aggregates. DLS was performed on the DNA-modified Au nanoparticles upon addition of the different length DNA linkers (**1**−**3**) to measure the initial growth rate of the aggregates. In this experiment, the conditions were analogous to those used in monitoring aggregation by UV−visible spectroscopy (vide supra). Interestingly, the aggregate growth rate is dependent on the length of the linker used, with the 48 and 72 base linked aggregates exhibiting significantly slower growth rates than the 24 base linked aggregates, Figure 7. The initial aggregation rates suggest that the sizes of the preannealed aggregates formed under these conditions are significantly different. However, the large size of the macroscopic precipitates formed with DNA linkers **1**−**3** is out of the range of DLS, which can only accurately size samples up to approximately 3 μm. As a result, a direct size measurement of the pre- and postannealed DNA-linked aggregates was not possible using this technique.

The rate of aggregate growth in this system is very complex and depends on a number of factors. Two critical factors are the rate of DNA linker binding to the complementary DNA attached to the surface of the gold nanoparticles (k_1), and the subsequent growth of the aggregates (k_2) via a DNA-modified particle with linker-attached hybridizing to a complementary DNA-modified particle, Scheme 4. It is expected that the longer 48 and 72 base linkers, which contain a duplex spacer portion, will exhibit slower diffusion rates[21] than the 24 base linker which will decrease the rate of DNA hybridization to the gold nanoparticles (k_1) thereby resulting in slower aggregate growth rates. Additionally, the slower aggregate growth rates (k_2)

(20) Park, S. J.; Lazarides, A. A.; Storhoff, J. J.; Mirkin, C. A.; Letsinger, R. L. Manuscript in preparation.

(21) Tinland, B.; Pluen, A.; Sturm, J.; Weill, G. *Macromolecules* **1997**, *30*, 5763−5765.

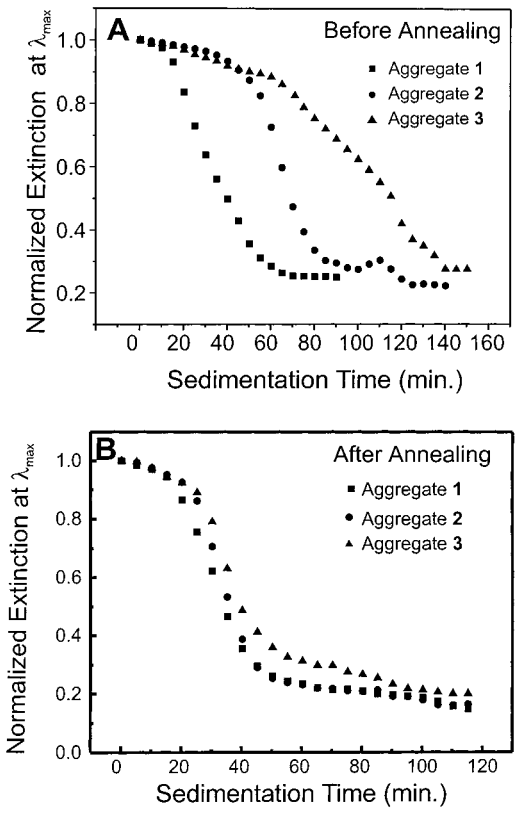

Figure 8. (A) Sedimentation rate measurement of the preannealed DNA-linked aggregates **1**−**3**. (B) Sedimentation rate measurement of the annealed DNA-linked aggregates (**1**−**3**). The sedimentation rate values (*S*) are given in Table 1.

associated with the longer duplex linkers (**2** and **3**) could be due in part to steric hindrance of nanoparticle aggregation. More specifically, both DNA-modified particles (**A** and **B**) have DNA linkers attached, which will sterically hinder the accessibility of the much shorter twelve base recognition strands as incoming complementary nanoparticle-DNA linkers try to bind, Scheme 4. The larger size of the longer DNA linkers (**2** and **3**) would be expected to sterically hinder the accessibility of the shorter recognition strands to a greater extent than the shorter 24 base linker effectively slowing down the aggregate growth rate (k_2).

Sedimentation Rates of the DNA-Linked Aggregates Before and After Annealing. To further analyze the aggregates containing the different length DNA linkers (**1**−**3**), sedimentation rates of the DNA-linked Au nanoparticle aggregates (state C for **1**−**3** in Scheme 2) were monitored by following the intensity of the plasmon band maximum in the visible spectrum of the aggregates as they settled out of solution. We have defined the parameter *S* as the value for the approximate sedimentation rate, which can be determined by taking the midpoint of the change in extinction at the plasmon maximum as aggregate sedimentation occurs. In this system, the two variables that affect the sedimentation rate are (1) the gold volume fraction as determined by interparticle distance and (2) the overall size (e.g. total mass) of the aggregate. The preannealed DNA-linked aggregates (**1**−**3**) exhibited significantly different sedimentation rates with values that were inversely dependent on the DNA linker length (S = 33, 65, and 106 min for linkers **1**, **2**, and **3**, respectively), Figure 8A and Table 1. The sedimentation rates of the preannealed DNA-linked aggregates likely reflect a difference in both the gold volume fraction as determined by the length of the different DNA linkers and the aggregate size, as kinetically determined by the different linkers. After annealing, the DNA-linked aggregates (**1**−**3**) exhibited similar sedimentation rates (S = 31, 32, and 35 min for linkers **1**, **2**, and **3**, respectively, Figure 8B and Table 1), regardless of linker length. As noted earlier, the SAXS data demonstrate that the interparticle distance of the 72 base linked aggregates does not change significantly after annealing. Therefore, the change in sedimentation rates of the annealed aggregates (**2** and **3**) must be due to a change in the size of the aggregates as predicted based on electrodynamics modeling of the optical properties. More specifically, annealing causes a disproportionately large increase in aggregate sizes for the 48 and 72 base linked structures as compared with the 24 base linked system.

TEM of the DNA-Linked Aggregates Before and After Annealing. TEM was used to analyze the size and structure of the pre- and postannealed DNA-linked aggregates (**1**−**3**), Figures 9 and 10. Two types of TEM images were recorded for each aggregate sample: one at low magnification to monitor size and density of the aggregates, and the other at higher magnification to determine the structural fate of the DNA-linked nanoparticles in the solid state. For the preannealed structures, the 24 base linked aggregates appear very large, dense, and multilayered (the extremely dark areas in Figure 9A,B), while the 48 and 72 base linked aggregates appear smaller and less densely packed, Figure 9C−E. By comparison, the postannealed structures (**1**−**3**) were large, dense, and virtually indistinguishable from each other, Figure 10. It is important to note that the SAXS data indicated that the interparticle distance does not change significantly upon annealing (vide supra). Therefore, the apparent densification of the annealed 48 and 72 base linked aggregates can be explained by an aggregate size increase, which results in the aggregates appearing much more dense when they are dried onto the TEM grid and imaged. Although there is some uncertainty about the exact relationship between these solid-state structures in UHV and their corresponding solution structures, it is clear that the preannealed 24 base linked aggregates contain a larger number of particles and are more dense than the 48 and 72 base linked aggregates, and that annealing in all three cases yields solution and solid-state structures that are virtually indistinguishable by TEM, UV−visible spectroscopy, and sedimentation rate. Based on these data in conjunction with SAXS and electrodynamic modeling, it is clear that significant increases in aggregate size occur for the 48 and 72 base linked structures during the annealing process and that aggregate size significantly influences the optical properties of the Au nanoparticle network materials. More specifically, it appears that for these systems many thousands of particles are required to achieve the maximum red shift in the plasmon bands for the aggregate structures.

Ostwald Ripening of DNA-Linked Aggregates. We liken the annealing process to an "Ostwald ripening" process where large aggregates, with smaller surface-to-bulk ratios (with respect to nanoparticles), grow at the expense of smaller aggregates, Scheme 5.[22] In this model, the melting properties of the particles at the surface of an aggregate will be more similar to normal duplex DNA than the particles in the interior of the aggregate. Like normal duplex DNA, the surface particles will have a broader melting transition and an earlier melting onset than interior particles with many DNA interconnects. Indeed, the breadth of the transition for duplex DNA **1** without nanoparticles (transition full width is ∼20 °C) is comparable

(22) Smith, A. *Particle Growth in Suspensions*; Academic Press: London, 1983.

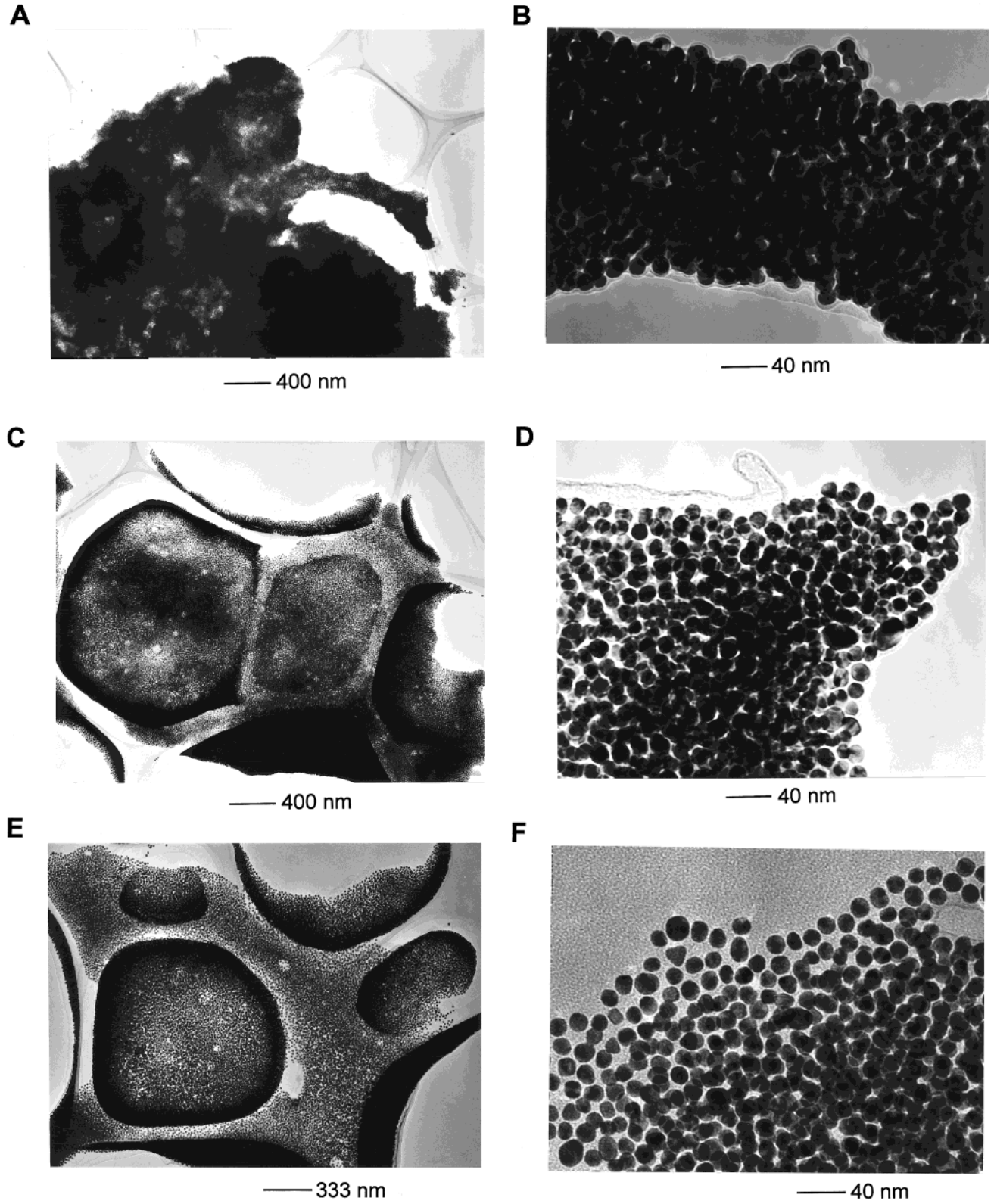

Figure 9. (A−F) TEM images of the preannealed DNA-linked aggregates **1**−**3**. (A) A portion of a 24 base linked aggregate **1**. (B) A higher magnification image of the area in part A. (C) A 48 base linked aggregate **2**. (D) A higher magnification image of the area in part C. (E) A 72 base linked aggregate **3**. (F) A higher magnification image of the area in part E. Scale bars for each image are shown at the bottom of the micrograph.

to the breadth of the transition involving the preannealed DNA linked aggregates (**3**), if the onset of the drop in extinction associated with Ostwald ripening (∼38 °C) is recorded as the starting point (transition full width is ∼19 °C), Figure 11. In accord with this, the drop in extinction at 260 nm and rise in extinction at 700 nm that is characteristic of preannealed structures (**2** and **3**) just before bulk aggregate dissociation is due to aggregate growth via an Ostwald ripening process. As a result, the postannealed aggregates (**2** and **3**) do not exhibit these temperature-dependent optical changes just before melting (no dip in extinction as in Figure 11) because the small aggregates already have been converted into larger aggregates, Figure 4.

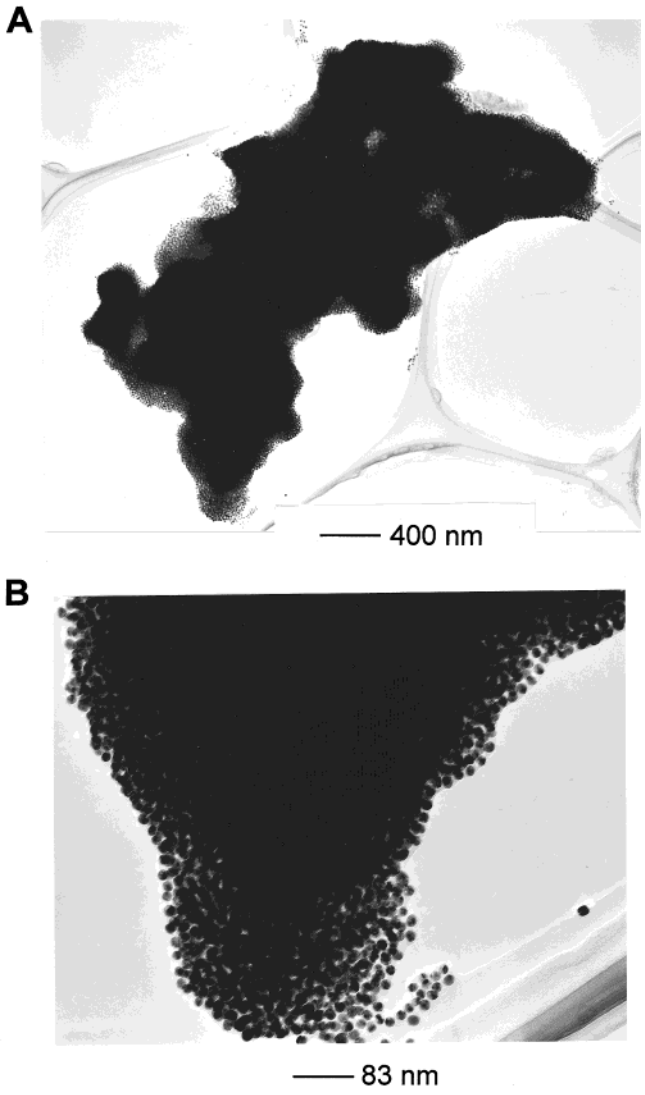

Figure 10. A representative TEM image of the annealed DNA-linked aggregates (**1**−**3**). Here, a 72 base linked aggregate (**3**) is shown at two different magnifications: (A) image of an entire aggregate on the micron scale; (B) higher magnification image of a portion of the aggregate in part A. Note that there are no dispersed particles.

In addition, they exhibit substantially narrower melting transitions (transition full width is ∼8 °C).

Conclusions

We have demonstrated that the optical properties of macroscopic DNA-linked Au nanoparticle aggregates can be controlled through choice of DNA linker length within these novel structures. Importantly, the optical differences observed for the DNA-linked aggregates formed with the different length oligonucleotide linkers are due not only to interparticle distance but also aggregate size (i.e. number of particles per aggregate structure). The different rates of DNA hybridization associated with the three oligonucleotide linkers in this system provide kinetic control over aggregate size and, therefore, the resulting optical properties. Annealing of the kinetic structures formed from the two longer oligonucleotide linkers at temperatures just below their melting points leads to significant optical changes. Electrodynamic modeling of the optical changes observed upon annealing show that these changes are more consistent with changes in aggregate size rather than interparticle distance. Furthermore, SAXS, sedimentation rates, and TEM are consistent with the electrodynamics modeling and also support a

Scheme 5

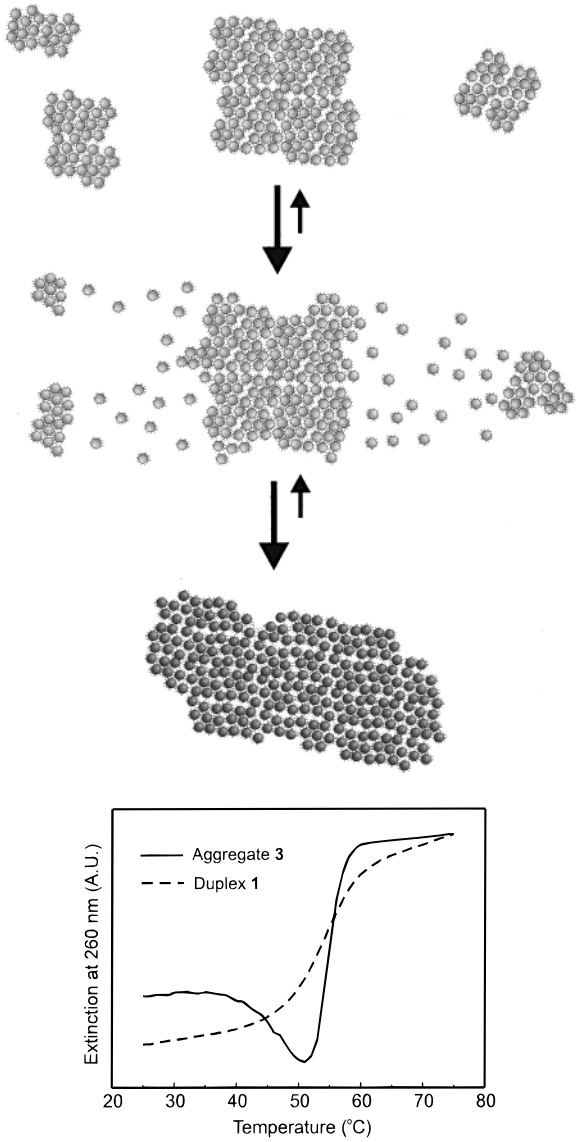

Figure 11. A comparison of thermal dissociation curves for the preannealed 72 base linked aggregates **3** and a 24 base duplex **1** (without nanoparticles). Note that the sequence for **1** is isosequential with the portion of the 72-base linker that initially melts in these experiments upon aggregate dissociation. The thermal dissociation of the 24 base DNA duplex and the aggregate dissociation profile of the 72 base linked aggregate (**3**) were monitored at 260 nm. The hybridization buffers were identical (0.3 M PBS), but the experiment involving the 24 base duplex was performed at a higher concentration (2.2 μM in each DNA strand) to obtain a measurable signal. Due to these concentration differences, the absolute melting temperatures may not be significant, but the breadth of the transitions are.

change in aggregate size upon annealing. The resulting annealed 48 and 72 base linked structures are comparable to the 24 base linked aggregate, with similar sedimentation rates, and virtually identical optical properties and melting behaviors. Interestingly, this suggests that with regard to the optical properties for these composite materials, DNA linkers might be more useful as kinetic controllers of aggregate growth than as spacer units. This also has significant ramifications with regard to the development of detection methods for DNA based on these novel nanoparticle materials and their aggregate size-dependent optical properties. Current work is aimed at exploiting these properties in the development of quantitative colorimetric assays for DNA.

Acknowledgment. We acknowledge the ARO (MURI DAAG 55-97-1-0133) (C.A.M., G.C.S.), the NIH (GM57356-02) (R.L.L., C.A.M.), and the NSF (CHE-9871903) (C.A.M., R.L.L., G.C.S.) for support of this research. The SAXS experiments were performed at the Dupont-Northwestern-Dow Collaborative Access Team (DND-CAT) Synchrotron Research Center located at Sector 5 of the Advanced Photon Source. DND-CAT is supported by E.I. Dupont de Nemours & Co., The Dow Chemical Company, the U.S. National Science Foundation through Grant DMR-9304725, and the State of Illinois through the Department of Commerce and the Board of Higher Education Grant IBHE HECA NWU 96. Use of the Advanced Photon Source was supported by the U.S. Department of Energy, Basic Energy Sciences, Office of Energy Research under Contract No. W-31-102-Eng-38. The authors also acknowledge the use of the Keck Biophysics Facility for the DLS measurements. The Keck facility is supported by the W. M Keck Foundation with additional support from NIH, The Rice Foundation, and the Robert H. Lurie Comprehensive Cancer Center. The authors also would like to acknowledge So Jung Park and Linette Demers for assistance with SAXS.

JA993825L